

Electronic band structure, Fermi surface, and elastic properties of polymorphs of the new 5.2K iron-free superconductor SrPt_2As_2 from first principles calculations

I. R. Shein * and A. L. Ivanovskii

*Institute of Solid State Chemistry, Ural Branch, Russian Academy of Sciences,
91, Pervomaiskaya St., Ekaterinburg, 620990 Russia*

ABSTRACT

By means of the first-principles calculations, we studied in detail the structural, elastic, and electronic properties of the new tetragonal CaBe_2Ge_2 -type 5.2K superconductor SrPt_2As_2 in comparison with two hypothetical SrPt_2As_2 polymorphs with ThCr_2Si_2 -type structures, which differ in the atomic configurations of $[\text{Pt}_2\text{As}_2]$ (or $[\text{As}_2\text{Pt}_2]$) blocks. We found that CaBe_2Ge_2 -type SrPt_2As_2 is a unique system with near-Fermi bands of a complicated character and an “intermediate”-type Fermi surface, which consists of electronic pockets having a cylinder-like (2D) topology (typical of 122 FeAs phases) together with 3D-like electronic and hole pockets, which are characteristic of ThCr_2Si_2 -like iron-free low- T_c superconductors. Our analysis revealed that as distinct from ThCr_2Si_2 -like 122 phases, other features of CaBe_2Ge_2 -like SrPt_2As_2 are as follows: (1). essential differences in contributions from $[\text{Pt}_2\text{As}_2]$ and $[\text{As}_2\text{Pt}_2]$ blocks to the near-Fermi region when conduction is anisotropic and occurs mainly in $[\text{Pt}_2\text{As}_2]$ blocks; (2). formation of a 3D system of strong covalent Pt-As bonds (inside and between $[\text{Pt}_2\text{As}_2]/[\text{As}_2\text{Pt}_2]$ blocks), which is responsible for enhanced stability of this polymorph; and (3). essential charge anisotropy between adjacent $[\text{Pt}_2\text{As}_2]$ and $[\text{As}_2\text{Pt}_2]$ blocks. We also predicted that CaBe_2Ge_2 -like SrPt_2As_2 is a mechanically stable and relatively soft material with high compressibility, which will behave in a ductile manner. On the contrary, the ThCr_2Si_2 -type SrPt_2As_2 polymorphs, which contain only $[\text{Pt}_2\text{As}_2]$ or $[\text{As}_2\text{Pt}_2]$ blocks, are less stable, have Fermi surfaces of a multi-sheet three-dimensional type like the ThCr_2Si_2 -like iron-free 122 phases, and therefore will be ductile materials with high elastic anisotropy. Based on our data for the three simplest SrPt_2As_2 polymorphs we assumed that there may exist a family of higher-order polytypes, which can be formed as a result of various stacking of the two main types of building blocks ($[\text{Pt}_2\text{As}_2]$ and $[\text{As}_2\text{Pt}_2]$) in various combinations along the z axis. This may provide an interesting platform for further theoretical and experimental search for new superconducting materials.

PACS : 71.18.+y, 71.15.Mb, 74.25.Jb

Keywords: Tetragonal SrPt_2As_2 polymorphs, Structural, electronic, elastic properties; *ab initio* calculations

I. INTRODUCTION

Among the broad family of recently discovered¹ iron-based superconductors (SCs), the so-called 122 phases²⁻⁹ belong to one of the most interesting and intensely studied groups of such materials. Their parent phases are $A\text{Fe}_2\text{As}_2$ (where A are alkali earth metals Ca, Sr, and Ba or Eu), which adopt a quasi-two-dimensional (2D) tetragonal crystal structure of the ThCr_2Si_2 -type, where $[\text{Fe}_2\text{As}_2]$ blocks are separated by A atomic sheets. In turn, inside $[\text{Fe}_2\text{As}_2]$ blocks, Fe ions form a square lattice sandwiched between two As sheets shifted so that each Fe is surrounded by a distorted As tetrahedron $\{\text{FeAs}_4\}$.

The most remarkable aspects of 122 SCs are as follows: (i) undoped $A\text{Fe}_2\text{As}_2$ phases exhibit a collinear antiferromagnetic (AF) spin density wave (SDW),^{2,5,10} (ii) superconductivity emerges owing to their hole or electron doping (or external pressure),²⁻⁹ and (iii) near-Fermi Fe $3d$ -like bands play an essential role in superconductivity.^{6,7,9}

Thus, the atomic substitutions inside $[\text{Fe}_2\text{As}_2]$ blocks exert a profound influence on the properties of these 122 phases, in particular, on their superconductivity. So, it was found that electron doping of $A\text{Fe}_2\text{As}_2$ phases as a result of partial substitution $M \rightarrow \text{Fe}$, where M are some magnetic or non-magnetic $3d$ - $5d$ metals of VIII group (Co, Ni, Pd, Ru, Rh, or Ir), induces superconductivity with T_c to ~ 20 K for such doped $A\text{Fe}_{2-x}M_x\text{As}_2$ phases.

The phase diagrams for such $A\text{Fe}_{2-x}M_x\text{As}_2$ systems usually show a SDW that competes with superconductivity; the onset of superconductivity coincides with a Lifshitz transition^{10,11} (change in the Fermi surface (FS) topology) and superconductivity generally appears¹²⁻¹⁶ in a broad window of M/Fe stoichiometry when the SDW is suppressed by doping. Besides, to gain a further insight into the nature of these systems, attention was paid also to the so-called "over-doped" limit, and a series of iron-free 122 phases $AM_2\text{As}_2$ ($M = \text{Co}, \text{Ni}, \text{Pd}, \text{Ru}, \text{Rh}, \text{or Ir}$) has been recently examined both experimentally and theoretically.¹⁷⁻²⁷ All these $AM_2\text{As}_2$ phases (such as SrNi_2As_2 , BaNi_2As_2 , SrRu_2As_2 , BaRu_2As_2 , SrRh_2As_2 , BaRh_2As_2 *etc.*) preserve the ThCr_2Si_2 -like type, but show very low transition temperatures ranging in the interval $T_c \sim 0.3 - 3.0\text{K}$.

In this context, of interest is the unusual situation for the systems A -(Fe/Pt)-As. Indeed, the diagrams of superconducting and magnetic phases in the Pt-substituted series $\text{BaFe}_{2-x}\text{Pt}_x\text{As}_2$ ^{28,29} and $\text{SrFe}_{2-x}\text{Pt}_x\text{As}_2$ ³⁰ (for which the maximal T_c to $\sim 23\text{K}$ and $\sim 16\text{K}$ was achieved at $x = 0.05$ ²⁹ and $x = 0.16$,³⁰ respectively) are similar to those for the above transition-metal-substituted $A\text{Fe}_2\text{As}_2$ systems. These Pt-doped systems also keep the ThCr_2Si_2 -like structure of initial $A\text{Fe}_2\text{As}_2$ phases.

On the contrary, the iron-free SrPt_2As_2 , which may be viewed as the fully Pt-substituted $A\text{Fe}_2\text{As}_2$ as compared with other known 122-like iron-free SCs, shows the maximal $T_c \sim 5.2\text{K}$ ³¹ and adopts^{31,32} a tetragonal CaBe_2Ge_2 -type structure. Thus, for SrPt_2As_2 we observed a very intriguing structural situation. Indeed, the structures for the above ThCr_2Si_2 -like $AM_2\text{As}_2$ may be described as a sequence of atomic sheets (along the c axis) $\dots-[\text{As}-M_2-\text{As}]-A-[\text{As}-M_2-\text{As}]-A-\dots$. On the contrary, for CaBe_2Ge_2 -like SrPt_2As_2 this sequence is: $\dots-[\text{As}-\text{Pt}_2-\text{As}]-\text{Sr}-[\text{Pt}-\text{As}_2-\text{Pt}]-\text{Sr}-[\text{As}-\text{Pt}_2-\text{As}]-\text{Sr}-\dots$, *i.e.* this structure contains $[\text{Pt}_2\text{As}_2]$ blocks where each Pt atom is surrounded by an As tetrahedron $\{\text{PtAs}_4\}$ alternating with $[\text{As}_2\text{Pt}_2]$ blocks consisting of $\{\text{AsPt}_4\}$ tetrahedrons. Thus, the new 5.2K iron-free superconductor SrPt_2As_2 cannot be considered as an analogue of the above ThCr_2Si_2 -like iron-free 122 phases $AM_2\text{As}_2$ ($M = \text{Co}, \text{Ni}, \text{Pd}, \text{Ru}, \text{Rh}, \text{or Ir}$).

In view of these circumstances, in the present work we performed the first-principles calculations to analyze the effects of the above unique structural features on the electronic and elastic properties for SrPt₂As₂.

The aim of this work was of two kinds. Firstly, we focused our attention on the peculiarities of electronic band structure, Fermi surface topology, and elastic properties for the recently synthesized^{31,32} 5.2K SC SrPt₂As₂ with a tetragonal CaBe₂Ge₂-type structure. Secondly, using SrPt₂As₂ as an example, we wanted to determine how the stability and some properties of 122-like phases are affected by local atomic arrangements inside [*M*-As] blocks, *i.e.* {*M*As₄} *versus* {As*M*₄}, and by various stacking of these blocks, when external atoms from neighboring blocks can form different types of inter-blocks bonds, namely, As-*M*, As-As or *M*-*M*.

For this purpose, three tetragonal SrPt₂As₂ polymorphs: the synthesized CaBe₂Ge₂-like phase and two hypothetical ThCr₂Si₂-like phases with alternative atomic configurations of [Pt₂As₂] (or [As₂Pt₂]) blocks, have been examined. As a result, the structural parameters, stability, electronic bands, FS topology, densities of states, and the peculiarities of inter-atomic interactions for the above polymorphs have been obtained and analyzed. In addition, the elastic parameters (independent elastic constants, bulk and shear moduli, indexes of elastic anisotropy) have been predicted for these polymorphs, and the Young's moduli, Poisson's ratio, and Pugh's indicator of brittle/ductile behavior for the corresponding polycrystalline systems (in the Voigt-Reuss-Hill approximation) have been evaluated.

II. MODELS AND COMPUTATIONAL ASPECTS

The synthesized^{31,32} SrPt₂As₂ crystallizes in a tetragonal CaBe₂Ge₂-type structure (space group P4/nmm, #129). The atomic positions are Sr: 2*c* (1/4, 1/4, *z*_{Sr}); 2*a* (3/4, 1/4, 0); Pt₂: 2*c* (1/4, 1/4, *z*_{Pt}); As1: 2*b* (3/4, 1/4, 1/2); and As2: 2*c* (1/4, 1/4, *z*_{As}), where *z*_{Sr,Pt,As} are the so-called internal coordinates. The structure of this phase (further denoted as SPA-I) can be schematically described as a sequence of Sr sheets and [Pt₂As₂] and [As₂Pt₂] blocks consisting of {PtAs₄} and {AsPt₄} tetrahedrons: ...[Pt₂As₂]/Sr/[As₂Pt₂]/Sr/[Pt₂As₂]/Sr/[As₂Pt₂]... as shown in Fig. 1.

We also examined two hypothetical tetragonal SrPt₂As₂ polymorphs with a ThCr₂Si₂-type structure (space group *I4/mmm*; #139). For one of them, denoted as SPA-II, the "conventional" ThCr₂Si₂-type structure was chosen, where the atomic positions are Sr: 2*a* (0, 0, 0), Pt: 4*d* (1/2, 0, 1/2) and As: 4*e* (0, 0, *z*_{As}); here, the stacking sequence is ...Sr/[Pt₂As₂]/Sr/[Pt₂As₂]/Sr... For the second hypothetical polymorph (abbreviated as SPA-III) we also used the ThCr₂Si₂ structural type, but with inverse distribution of Pt and As over the atomic sites (in blocks) as compared with SPA-II, *i.e.* the atomic positions here are: Sr: 2*a* (0, 0, 0), As: 4*d* (1/2, 0, 1/2) and Pt: 4*e* (0, 0, *z*_{Pt}). The stacking sequence for SPA-III is ... Sr/[As₂Pt₂]/[As₂Pt₂]/Sr..., see Fig. 1.

As a result, three basic tetragonal types of SrPt₂As₂ polymorphs have been examined, which enable us to clarify the role of (i) local atomic arrangement inside [Pt-As] blocks, *i.e.* {PtAs₄} *versus* {AsPt₄}, and of (ii) the main types of stacking of these blocks, *i.e.* ...[Pt₂As₂]/Sr/[As₂Pt₂]/Sr/[Pt₂As₂]/Sr/[As₂Pt₂]... *versus* ...Sr/[Pt₂As₂]/Sr/[Pt₂As₂]/Sr... *versus* ...Sr/[As₂Pt₂]/[As₂Pt₂]/Sr..., when the external atoms from neighboring blocks can form various inter-blocks bonds, namely, As-Pt, As-As, and Pt-Pt, respectively.

Our band-structure calculations were carried out by means of the full-potential method with mixed basis APW+lo (LAPW) implemented in the WIEN2k suite of programs.³³ The generalized gradient correction (GGA) to exchange-correlation potential in the PBE form³⁴ was used. The plane-wave expansion was taken to $R_{\text{MT}} \times K_{\text{MAX}}$ equal to 8, and the k sampling with $14 \times 14 \times 14$ k -points in the Brillouin zone was used. The MT sphere radii were chosen to be 2.3 a.u. for Pt, 2.5 a.u. for Sr, and 1.9 a.u. for As. The calculations were performed with full-lattice optimization including internal coordinates. The self-consistent calculations were considered to be converged when the difference in the total energy of the crystal did not exceed 0.1 mRy and the difference in the total electronic charge did not exceed 0.001 e as calculated at consecutive steps. On the example of SPA-I we have examined the influence of relativistic effects (the spin-orbital interactions (SOC) within FLAPW) on the valence bands and FS. It was found that SOC mainly results in energy shift and splitting of core and semi-core Pt states, which lay deeply under Fermi's level, whereas the common picture of valence bands (as well as the DOSs distributions and FS topology) as obtained in our calculations without SOC and within spin-orbit coupling varies very little. Thus further in all our calculations a standard procedure of electronic structure calculation and elastic properties in a scalar-relativistic approximation was used.

The hybridization effects were analyzed using the densities of states (DOSs), which were obtained by the modified tetrahedron method.³⁵ The ionic bonding was considered using Bader³⁶ analysis. In this approach, each atom of a crystal is surrounded by an effective surface that runs through minima of the charge density, and the total charge of an atom (the so-called Bader charge, Q^{B}) is determined by integration within this region. In addition, some peculiarities of intra-atomic bonding picture were visualized by means of charge density maps.

Furthermore, for the calculations of the elastic parameters of the considered SrPt_2As_2 polymorphs we employed the Vienna *ab initio* simulation package (VASP) in projector augmented waves (PAW) formalism.^{37,38} Exchange and correlation were described by a nonlocal correction for LDA in the form of GGA.³⁴ The kinetic energy cutoff of 500 eV and k -mesh of $14 \times 14 \times 7$ were used. The geometry optimization was performed with the force cutoff of 1 meV/Å.

These two DFT-based codes are complementary and allowed us to perform a complete investigation of the declared properties of the above systems.

III. RESULTS AND DISCUSSION

A. Structural properties and stability

As the first step, the total energy (E_{tot}) *versus* cell volume calculations were carried out to determine the equilibrium structural parameters for the considered SrPt_2As_2 polymorphs. The calculated values are presented in Table I and are in reasonable agreement with the available experiments.^{31,32} Some divergences are related to the well-known overestimation of the lattice parameters within LDA-GGA based calculation methods.

For the CaBe_2Ge_2 -type polymorph (SPA-I), the Pt-As bond lengths (2.52 Å) between neighboring $[\text{Pt}_2\text{As}_2]/[\text{As}_2\text{Pt}_2]$ blocks are comparable with those for the Pt-As lengths (about 2.6 Å) inside these blocks. Thus, this polymorph may be viewed as a quite isotropic phase with a three-dimensional (3D) system of strong Pt-As bonds. On the

contrary, for the ThCr_2Si_2 -type polymorphs (SPA-II and SPA-III, where the external planes are formed by As (or Pt) atoms within $[\text{As}_2\text{Pt}_2]$ (or $[\text{Pt}_2\text{As}_2]$) blocks, respectively) the nearest As-As (or Pt-Pt) distances between neighboring blocks are twice smaller than the corresponding inter-atomic distances inside the blocks. On the other hand, for both polymorphs the Pt-As lengths inside $[\text{As}_2\text{Pt}_2]$ (or $[\text{Pt}_2\text{As}_2]$) blocks are comparable with those for SPA-I, Table I. Thus, these simple crystallographic reasons allow us to expect that in contrast to SPA-I with a 3D system of Pt-As bonds, the bonding for SPA-II and SPA-III should be very anisotropic: simultaneously with Pt-As bonds inside the blocks, direct As-As (for SPA-II) or Pt-Pt bonds (for SPA-III) will be formed between the corresponding blocks, see also below.

Let us note also that the calculated bond angles Pt-As-Pt and As-Pt-As in tetrahedrons $\{\text{PtAs}_4\}$ and $\{\text{AsPt}_4\}$ for all of the SrPt_2As_2 polymorphs, see Table II, are far from the ideal tetrahedron angle (109.5°), which is considered as a factor favorable for superconductivity in FeAs systems.⁶⁻⁹

Next, the total-energy differences (ΔE) between the examined SrPt_2As_2 polymorphs are summarized in Table I. The results reveal that both within the FLAPW and VASP approaches the most stable and unstable polymorphs are, respectively, SPA-I with the CaBe_2Ge_2 -like structure and SPA-II with a “conventional” ThCr_2Si_2 -type lattice.

B. Electronic band structure and Fermi surface

The calculated band structure and electronic densities of states (DOS) for the considered SrPt_2As_2 polymorphs are shown in Figs. 2 and 3, respectively. For all the polymorphs, their electronic spectra show some common features, namely (i) the As $4p$ states occur between -7 eV and -4 eV with respect to the Fermi energy ($E_F = 0$ eV); (ii) most of the bands between -4 eV and E_F are mainly of the Pt $5d$ character, and (iii) the contributions from the valence states of Sr to the occupied bands are quite small. However, in the vicinity of the Fermi energy the topology of the electronic bands for various SrPt_2As_2 polymorphs becomes completely different.

So, for the synthesized CaBe_2Ge_2 -like phase these near-Fermi bands demonstrate (Fig. 2) a unique complicated “mixed” character: simultaneously with quasi-flat bands along R-X, a series of high-dispersive Pt $5d$ - like bands intersects the Fermi level between Γ and Z points and in the A-Z direction. These features yield an unusual multi-sheet FS, Fig. 4. Indeed, the Fermi surface of CaBe_2Ge_2 -like SrPt_2As_2 consists of a set of hole and electronic sheets, where two electron-like pockets at the corners (around M) have a cylinder-like (2D) topology, and are very similar to the related electron cylinders along the k_z direction at the zone corners obtained for ThCr_2Si_2 -like $A\text{Fe}_2\text{As}_2$ materials.^{6,7,39-42} However, the two other sheets (around Γ – electronic and hole-like sheets, see Fig. 5) are of a three-dimensional type similar to those for ThCr_2Si_2 -like iron-free low- T_c SCs such as SrNi_2As_2 , SrRu_2As_2 , BaRu_2As_2 , SrRh_2As_2 , *etc.*^{23,24,43-45}

On the contrary, the Fermi surfaces of both ThCr_2Si_2 -like SrPt_2As_2 polymorphs differ essentially from those of the FeAs-based 122 materials and are of a characteristic multi-sheet three-dimensional type like the above ThCr_2Si_2 -like iron-free $AM_2\text{As}_2$ phases,^{23,24,43-45} see Fig. 4.

As electrons near the Fermi surface are involved in the formation of the superconducting state, it is important to understand their nature. The total, atomic, and orbital decomposed partial DOSs at the Fermi level, $N(E_F)$, are shown in Table III. It is seen that for all SrPt_2As_2 polymorphs the main contribution to $N(E_F)$ comes from the Pt

$5d$ states, with some additions of the As $4p$ states. For the examined polymorphs, the values of $N(E_F)$ decrease in the sequence: SPA-I > SPA-II > SPA-III, whereas the contributions of (As $4p$)/(Pt $5d$) states to $N(E_F)$ are: 0.303 (SPA-I) \sim 0.301 (SPA-II) < 0.370 (SPA-III).

The obtained data also allowed us to estimate the Sommerfeld constants (γ) and the Pauli paramagnetic susceptibility (χ) for SrPt₂As₂ polymorphs under the assumption of the free electron model as $\gamma = (\pi^2/3)N(E_F)k_B^2$ and $\chi = \mu_B^2N(E_F)$, Table III.

Note also that for the CaBe₂Ge₂-type SrPt₂As₂ polymorph (SPA-I) the contributions to $N(E_F)$ from the states of various blocks ([Pt₂As₂] *versus* [As₂Pt₂]) differ appreciably. Though the contributions of As1 $4p$ and As2 $4p$ states to $N(E_F)$ are quite small and comparable, the value of $N^{Pt1d}(E_F) = 0.59$ states/eV·atom for Pt1 atoms (placed inside [Pt₂As₂] blocks) is twice greater than $N^{Pt2d}(E_F) = 0.30$ states/eV·atom for Pt2 atoms located on the outer sides of [As₂Pt₂] blocks, see Fig. 3. Therefore, the conduction in SPA-I is expected to be most anisotropic, *i.e.* happening mainly in the [Pt₂As₂] blocks. To confirm this statement, we have calculated (within the FLMT0 approach ⁴⁶) Fermi velocity of the carriers along different directions, $\langle v_{x,y,z}^2 \rangle^{1/2}$, for SrPt₂As₂ polymorphs, which together with the values of $\langle v_{x,y,z}^2 \rangle^{1/2}$ for some others layered SCs are presented in Table IV. We see that the ratio $\langle v_{x,y}^2 \rangle^{1/2} / \langle v_z^2 \rangle^{1/2}$ is maximal for SPA-I (1.52) - in comparison with SPA-II (1.03) and SPA-III (1.08), testifying the largest anisotropy of this system among examined polymorphs.

For 5.2K SC SrPt₂As₂, the experimental value of $\gamma^{\text{exp}} = 9.72$ mJ·K⁻²·mol⁻¹ has been evaluated ³¹ from standard analysis of specific heat $C(T)$ measurements. This allowed us to estimate the average electron-phonon coupling constant λ for SrPt₂As₂ as $\gamma^{\text{exp}} = \gamma^{\text{theor}}(1 + \lambda)$. Within this crude estimation, the calculations yield $\lambda \sim 0.62$, *i.e.* SrPt₂As₂ may be classified as a conventional phonon-mediated superconductor within a moderate coupling limit. For comparison, the available estimations of λ for other related iron-free low-temperature 1111 and 122 SCs are about 0.58 (for LaNiPO ⁴⁹) or 0.76 (for BaNi₂As₂ ⁴⁴).

C. Inter-atomic bonding

A conventional picture of inter-atomic interactions in ThCr₂Si₂-like AM_2As_2 phases assumes strong M -As bonding of a mixed ionic-covalent type inside [M_2As_2] blocks, some covalent As-As interactions between the adjacent [M_2As_2]/[M_2As_2] blocks together with ionic bonding between [M_2As_2] blocks and atomic A sheets. ^{4,6-9,23,24,27,42,50,51} This bonding anisotropy determines the quasi-two-dimensional nature of these systems.

In our case, the overall character of **covalent Pt-As bonding** in SrPt₂As₂ polymorphs **inside** [Pt₂As₂] (or [As₂Pt₂]) blocks may be understood from site-projected DOS calculations. As is shown in Fig. 3, Pt $5d$ and As $4p$ states are strongly hybridized. In addition, the unoccupied levels (Pt $6p$ and As $3d$) in the examined phases become partially occupied and will hybridized with others valence states, but their contributions in the valence band (and in covalent bonding) are quite small. On the other hand, a completely different bonding in the examined polymorphs arises **between** the adjacent blocks, and this situation is clearly visible in Fig. 6. So, while for CaBe₂Ge₂-like SrPt₂As₂ strong covalent Pt-As bonding takes place, for the hypothetical ThCr₂Si₂-like polymorphs the directed unipolar As-As (SPA-II) or Pt-Pt bonds (SPA-III) appear. Thus, it is possible to assume that this 3D system of strong covalent Pt-As bonds, which appear inside and between [Pt₂As₂]/[As₂Pt₂] blocks for CaBe₂Ge₂-like SrPt₂As₂, is responsible for enhanced stability of this polymorph.

In turn, for AM_2As_2 phases the *ionic bonding* is often explained^{6-9,42,50} within the oversimplified ionic model. In our case, if we assume the usual oxidation numbers of atoms: Sr^{2+} , Pt^{2+} , and As^{3-} , the charge distributions for $SrPt_2As_2$ should be +2 for Sr sheets and -2 for $[Pt_2As_2]$ ($[As_2Pt_2]$) blocks. Thus, for all $SrPt_2As_2$ polymorphs: (i) both types of $[Pt_2As_2]$ or $[As_2Pt_2]$ blocks should adopt the same ionic states (2-), and (ii) the identical charge transfer ($2e$) occurs from Sr^{2+} sheets to $[Pt_2As_2]^{2-}$ ($[As_2Pt_2]^{2-}$) blocks.

The real picture of charge distributions appears more complicated. To estimate numerically the amount of electrons redistributed between various atoms and between adjacent $[Pt_2As_2]^{n+}$ ($[As_2Pt_2]^{m+}$) blocks, we carried out a Bader³⁶ analysis. The total charge of an atom (the so-called Bader charge, Q^B), the corresponding charges as obtained from the purely ionic model (Q^i), and their differences ($\Delta Q = Q^B - Q^i$) are presented in Table V. The results confirm that all $SrPt_2As_2$ polymorphs are partly ionic compounds, and charges are transferred from Pt and Sr to As. Then, the effective charges for $[Pt_2As_2]$ ($[As_2Pt_2]$) blocks were found: $[Pt_2As_2]^{0.996-}$ versus $[As_2Pt_2]^{0.204-}$ for SPA-I, $[Pt_2As_2]^{0.578-}$ for SPA-II, and $[As_2Pt_2]^{0.576-}$ for SPA-III. Thus, in SPA-II and SPA-III we observed a quite identical charge transfer ($\delta \sim 0.6e$) from $Sr^{\delta+}$ sheets to $[Pt_2As_2]^{\delta-}$ ($[As_2Pt_2]^{\delta-}$) blocks. For SPA-I, on the contrary, essential charge anisotropy was obtained between adjacent $[Pt_2As_2]^{0.996-}/[As_2Pt_2]^{0.204-}$ blocks. Let us note that for $CaBe_2Ge_2$ -type $SrPt_2As_2$ the distribution of non-equivalent ionic $[Pt_2As_2]^{0.996-}/[As_2Pt_2]^{0.204-}$ blocks around the $Sr^{\delta+}$ sheets is a quite rare situation, which takes place, for example, for another related low- T_c SC – a layered phase $La_3Ni_4P_4O_{20}$ ^{52,53} with asymmetric distribution of ionic blocks around conducting $[Ni_2P_2]$ blocks.

D. Elastic properties

Let us discuss the elastic parameters for the examined $SrPt_2As_2$ polymorphs as obtained within VASP calculations. The standard “volume-conserving” technique was used in the calculation of stress tensors on strains applied to the equilibrium structure to obtain the elastic constants C_{ij} .⁵⁴ In this way the values of six independent elastic constants for tetragonal crystals (C_{11} , C_{12} , C_{13} , C_{33} , C_{44} and C_{66}) were estimated, Table VI.

First of all, C_{ij} constants for all $SrPt_2As_2$ polymorphs are positive and satisfy the generalized criteria⁵⁵ for mechanically stable tetragonal materials: $C_{11} > 0$, $C_{33} > 0$, $C_{44} > 0$, $C_{66} > 0$, $(C_{11}-C_{12}) > 0$, $(C_{11}+C_{33}-2C_{13}) > 0$, and $[2(C_{11}+C_{12})+C_{33}+4C_{13}] > 0$. Note that for SPA-II the value of C_{66} is very small. Thus, this polymorph (which is also energetically less favorable than SPA-I and SPA-III, according to total-energy calculations, Table I) lies on the border of mechanical stability.

Further, the calculated elastic constants C_{ij} allowed us to obtain the bulk (B) and shear (G) moduli. Usually, for such calculations two main approximations are used, namely the Voigt (V) and Reuss (R) schemes, see for example Ref. [56]. So, in the Voigt approximation, these parameters are:

$$B_V = [2(C_{11} + C_{12}) + C_{33} + 4C_{13}]/9,$$

$$G_V = [M + 3C_{11} - 3C_{12} + 12C_{44} + 6C_{66}]/30,$$

in Reuss approximation:

$$B_R = C^2/M,$$

$$G_R = 15 \{ (18B_V/C^2) + [6/(C_{11} - C_{12})] + (6/C_{44}) + (3/C_{66}) \}^{-1},$$

where $M = C_{11} + C_{12} + 2C_{33} - 4C_{13}$, and $C^2 = (C_{11} + C_{12})C_{33} - 2C_{13}^2$.

We evaluated also the corresponding parameters for polycrystalline SrPt₂As₂ species, *i.e.* for materials in the form of aggregated mixtures of microcrystallites with random orientation. For this purpose we utilized the Voigt-Reuss-Hill (VRH) approximation.⁵⁷⁻⁵⁹ In this approach, the actual effective moduli (B_{VRH} and G_{VRH}) for polycrystals are approximated by the arithmetic mean of the two above mentioned limits - Voigt and Reuss and further allowed us to obtain the Young's moduli Y and the Poisson's ratio ν as: $Y_{\text{VRH}} = 9 B_{\text{VRH}} / \{1 + (3B_{\text{VRH}}/G_{\text{VRH}})\}$, and $\nu = (3B_{\text{VRH}} - 2G_{\text{VRH}}) / 2(3B_{\text{VRH}} + G_{\text{VRH}})$.

The above elastic parameters are presented in Table VII and allow us to make the following conclusions:

(i). The bulk moduli of the SrPt₂As₂ polymorphs increase in the sequence: $B(\text{SPA-II}) < B(\text{SPA-III}) < B(\text{SPA-I})$. As the bulk modulus represents the resistance to volume change against external forces, this indicates that the highest average bond strength will be achieved for SPA-I. On the other hand, the obtained bulk modulus for SPA-I is quite small (~ 100 GPa), and therefore the recently discovered 5.2K SC SrPt₂As₂ should be classified as a relatively soft material with high compressibility ($\beta \sim 0.01$ GPa⁻¹). In addition, the Young's modulus of materials is defined as a ratio of linear stress and linear strain, which tells about their stiffness. The Young's modulus of CaBe₂Ge₂-type SrPt₂As₂ was found to be $Y \sim 72$ GPa; thus, this material will show a rather small stiffness.

(ii). For all SrPt₂As₂ polymorphs it was found that $B > G$; this implies that the parameter limiting the mechanical stability of these materials is the shear modulus G , which represents the resistance to shear deformation against external forces.

(iii). One of the most widely used malleability measures of materials is the Pugh's criterion (G/B ratio).⁶⁰ As is known empirically, if $G/B < 0.5$, a material behaves in a ductile manner, and *vice versa*, if $G/B > 0.5$, a material demonstrates brittleness. In our case, according to this indicator (Table VII), SrPt₂As₂ polymorphs will behave as ductile materials.

(iv). Elastic anisotropy of crystals reflects a different bonding character in different directions and has an important implication since it correlates with the possibility to induce microcracks in materials.^{61,62} We have estimated the elastic anisotropy for the examined materials using the so-called universal anisotropy index⁶³ defined as: $A^{\text{U}} = 5G_{\text{V}}/G_{\text{R}} + B_{\text{V}}/B_{\text{R}} - 6$. For isotropic crystals $A^{\text{U}} = 0$; the deviations of A^{U} from zero define the extent of crystal anisotropy. In our case, the minimal anisotropy is exhibited by 3D-like SPA-I, while SPA-II and SPA-III demonstrate the maximal (and comparable) deviations from $A^{\text{U}} = 0$ (Table VII) that testify to their high elastic anisotropy.

Finally, let us note that the elastic parameters of the 3D-like SPA-I polymorph (*i.e.* the synthesized 5.2K SC SrPt₂As₂ with a tetragonal CaBe₂Ge₂-type structure) are higher than those for ThCr₂Si₂-type FeAs phases. So, according to the available experimental and theoretical data, the bulk moduli are $B \sim 62$ GPa,⁶⁴ for SrFe₂As₂ and $B \sim 60$ GPa⁶⁵ for CaFe₂As₂ *versus* $B \sim 100$ GPa for CaBe₂Ge₂-type SrPt₂As₂ as obtained by us within VASP calculations. However, as a whole the elastic properties of 5.2K SC SrPt₂As₂ are comparable with the same for some other related FeAs SC's. So, the bulk moduli for 111 and 1111 FeAs SCs vary in the interval from ~ 57 GPa (for LiFeAs⁶⁶) to $\sim 100\div 120$ GPa for some 1111 FeAs phases such as LaFeAsO or NdFeAsO.⁶⁴⁻⁶⁹

IV. CONCLUSIONS

In summary, by means of the first-principles calculations we studied in detail the structural, elastic, and electronic properties of the new low-temperature superconductor –

tetragonal CaBe_2Ge_2 -type SrPt_2As_2 – in comparison with two hypothetical SrPt_2As_2 polymorphs with ThCr_2Si_2 -type structures, which differ in the atomic configurations of $[\text{Pt}_2\text{As}_2]$ (or $[\text{As}_2\text{Pt}_2]$) blocks.

Our studies showed that CaBe_2Ge_2 -type SrPt_2As_2 is a unique system with near-Fermi bands of a complicated “mixed” character: simultaneously with quasi-flat bands a set of high-dispersive bands intersects the Fermi level. The Fermi surface of this phase adopts an “intermediate” character and consists of electronic pockets having a cylinder-like (2D) topology (typical of 122 FeAs phases) together with 3D-like electronic and hole pockets, which are characteristic of ThCr_2Si_2 -like iron-free low- T_c SCs such as SrNi_2As_2 , SrRu_2As_2 , SrRh_2As_2 , *etc.* Next, the main contribution to $N(E_F)$ comes from the Pt 5d states, with some additions of the As 4p states, but these contributions from the states of $[\text{Pt}_2\text{As}_2]$ blocks are almost twice greater than from the $[\text{As}_2\text{Pt}_2]$ blocks. Thus, conduction in CaBe_2Ge_2 -type SrPt_2As_2 is expected to be anisotropic and happening mainly in $[\text{Pt}_2\text{As}_2]$ blocks.

Further, in contrast to ThCr_2Si_2 -like 122 phases, another feature of CaBe_2Ge_2 -like SrPt_2As_2 is the type of intra-atomic bonding. Here, (1). a 3D system of strong covalent Pt-As bonds (inside and between $[\text{Pt}_2\text{As}_2]/[\text{As}_2\text{Pt}_2]$ blocks) appears, which is responsible for enhanced stability of this polymorph, and (2). essential charge anisotropy was obtained between the adjacent $[\text{Pt}_2\text{As}_2]$ and $[\text{As}_2\text{Pt}_2]$ blocks. Finally, our analysis shows that the synthesized CaBe_2Ge_2 -like SrPt_2As_2 is a mechanically stable and relatively soft material with high compressibility ($\beta \sim 0.01 \text{ GPa}^{-1}$), which will behave in a ductile manner. However, this system will show the minimal anisotropy and an enhanced bulk modulus as compared with the examined ThCr_2Si_2 -like polymorphs and other isostructural 122 phases.

In turn, the considered hypothetical tetragonal SrPt_2As_2 polymorphs with a ThCr_2Si_2 -type structure, which contain only $[\text{Pt}_2\text{As}_2]$ or $[\text{As}_2\text{Pt}_2]$ blocks, are less stable. This fact can be explained taking into account the anisotropy of intra- and inter-blocks bonding, where alongside with Pt-As intra-blocks bonds, a system of unipolar As-As (or Pt-Pt) inter-blocks bonds appears. The Fermi surfaces of both ThCr_2Si_2 -like SrPt_2As_2 polymorphs differ essentially from those of the CaBe_2Ge_2 -like phase and are of a multi-sheet three-dimensional type like the above ThCr_2Si_2 -like iron-free $AM_2\text{As}_2$ phases. Finally, our analysis reveals that these ThCr_2Si_2 -like polymorphs will be ductile materials with high elastic anisotropy.

In conclusion, our calculations indicate that the difference in the ground-state energies of the examined SrPt_2As_2 phases is rather small. This allows us to speculate about the existence of a family of higher-order polytypes, which can be formed (by keeping the tetragonal type of the lattice) only as a result of various stacking of two main types of building blocks (“direct” $[\text{Pt}_2\text{As}_2]$ blocks formed from tetrahedrons $\{\text{PtAs}_4\}$ and “inverse” $[\text{As}_2\text{Pt}_2]$ blocks formed from tetrahedrons $\{\text{AsPt}_4\}$) in various combinations along the z axis. We also assume a possibility of polytypism for other related 122 phases. These systems can provide an interesting platform for further theoretical and experimental search for new superconducting materials. Another aspect, which calls for further studies, is the effect of structure³² modulation on the electronic properties of SrPt_2As_2 .

ACKNOWLEDGMENTS

This work was supported by the Russian Foundation for Basic Research, Grants No. RFBR- 09-03-00946 and No. RFBR- 10-03-96008.

* shein@ihim.uran.ru

- ¹ Y. Kamihara, T. Watanabe, M. Hirano, and H. Hosono, *J. Am. Chem. Soc.* **30**, 3296 (2008).
- ² M. Rotter, M. Tegel, and D. Johrendt, *Phys. Rev. Lett.* **101**, 107006 (2008).
- ³ M. Rotter, M. Tegel, D. Johrendt, I. Schellenberg, W. Hermes, and R. Pöttgen, *Phys. Rev. B* **78**, 020503 (R) (2008).
- ⁴ D. Kasinathan, A. Ormeci, K. Koch, U. Burkhardt, W. Schnelle, A. Leithe-Jasper and H. Rosner, *New J. Phys.* **11**, 025023 (2009)
- ⁵ C. Krellner, N. Caroca-Canales, A. Jesche, H. Rosner, A. Ormeci, and C. Geibel, *Phys. Rev. B* **78**, 100504 (R) (2008).
- ⁶ M. V. Sadovskii, *Physics-Uspekhi* **51**, 1201 (2008).
- ⁷ A. L. Ivanovskii, *Physics-Uspekhi* **51**, 1229 (2008).
- ⁸ H. Hiramatsu, T. Kamiya, M. Hirano, and H. Hosono, *Physica C* **469**, 657 (2009).
- ⁹ P. C. Canfield and S. L. Bud'ko, *Ann. Rev. Cond. Matter Phys.* **1**, 27 (2010).
- ¹⁰ E. D. Mun, S. L. Bud'ko, N. Ni, A. N. Thaler, and P. C. Canfield, *Phys. Rev. B* **80**, 054517 (2009)
- ¹¹ C. Liu, T. Kondo, R. M. Fernandes, A. D. Palczewski, E. D. Mun, N. Ni, A. N. Thaler, A. Bostwick, E. Rotenberg, J. Schmalian, S. L. Bud'ko, P. C. Canfield, and A. Kaminski, *Nat. Phys.* **6**, 419 (2010).
- ¹² S. R. Saha, N. P. Butch, K. Kirshenbaum, and J. Paglione, *Phys. Rev. B* **79**, 224519 (2009).
- ¹³ F. Han, X. Zhu, P. Cheng, G. Mu, Y. Jia, L. Fang, Y. Wang, H. Luo, B. Zeng, B. Shen, L. Shan, C. Ren, and H. H. Wen, *Phys. Rev. B* **80**, 024506 (2009).
- ¹⁴ W. Schnelle, A. Leithe-Jasper, R. Gumeniuk, U. Burkhardt, D. Kasinathan, and H. Rosner, *Phys. Rev. B* **79**, 214516 (2009).
- ¹⁵ A. Leithe-Jasper, W. Schnelle, C. Geibel, and H. Rosner, *Phys. Rev. Lett.* **101**, 207004 (2008).
- ¹⁶ N. Ni, A. Thaler, A. Kracher, J. Q. Yan, S. L. Bud'ko, and P. C. Canfield, *Phys. Rev. B* **80**, 024511 (2009).
- ¹⁷ A. Hellmann, A. Löhken, A. Wurth, and A. Mewis, *Z. Naturforsch.* **62b**, 155 (2007).
- ¹⁸ T. Mine, H. Yanagi, T. Kamiya, Y. Kamihara, M. Hirano, and H. Hosono, *Solid State Commun.* **147**, 111 (2008).
- ¹⁹ F. Ronning, N. Kurita, E.D. Bauer, B. L. Scott, T. Park, T. Klimczuk, R. Movshovich, and J. D. Thompson, *J. Phys.: Cond. Matter* **20**, 342203 (2008).
- ²⁰ E. D. Bauer, F. Ronning, B. L. Scott, and J. D. Thompson, *Phys. Rev. B* **78**, 172504 (2008).
- ²¹ R. Nath, Y. Singh, and D. C. Johnston, *Phys. Rev. B* **79**, 174513 (2009).
- ²² Y. Singh, Y. Lee, S. Nandi, A. Kreyssig, A. Ellern, S. Das, R. Nath, B. N. Harmon, A. I. Goldman, and D. C. Johnston, *Phys. Rev. B* **78**, 104512 (2008).
- ²³ I. R. Shein, and A. L. Ivanovskii, *Solid State Commun.* **149**, 1860 (2009).
- ²⁴ I. R. Shein, and A. L. Ivanovskii, *Phys. Rev. B* **79**, 054510 (2009).
- ²⁵ Z. G. Chen, G. Xu, W. Z. Hu, X. D. Zhang, P. Zheng, G. F. Chen, J. L. Luo, Z. Fang, and N. L. Wang, *Phys. Rev. B* **80**, 094506 (2009).
- ²⁶ N. Kurita, F. Ronning, Y. Tokiwa, E. D. Bauer, A. Subedi, D. J. Singh, J. D. Thompson, and R. Movshovich, *Phys. Rev. Lett.* **102**, 147004 (2009).
- ²⁷ I. R. Shein, and A. L. Ivanovskii, *Phys. Solid State*, **52**, 6 (2010).
- ²⁸ S. R. Saha, T. Drye, K. Kirshenbaum, N. P. Butch, P. Y. Zavalij, and J. Paglione, *J. Phys.: Condens. Matter* **22**, 072204 (2010).
- ²⁹ X. Zhu, F. Han, G. Mu, P. Cheng, J. Tang, J. Ju, K. Tanigaki, and H. H. Wen, *Phys. Rev. B* **81**, 104525 (2010).
- ³⁰ K. Kirshenbaum, S. R. Saha, T. Drye, and J. Paglione, *Phys. Rev. B* **82**, 144518 (2010).
- ³¹ K. Kudo, Y. Nishikubo, and M. Nohara, arXiv:1010.3950 (unpublished).

- ³² A. Imre, A. Hellmann, G. Wenski, J. Graf, D. Johrendt, and A. Mewis, *Z. Anorg. Allg. Chem.* **633**, 2037 (2007).
- ³³ P. Blaha, K. Schwarz, G. K. H. Madsen, D. Kvasnicka, and J. Luitz, *WIEN2k, An Augmented Plane Wave Plus Local Orbitals Program for Calculating Crystal Properties*, (Vienna University of Technology, Vienna, 2001)
- ³⁴ J. P. Perdew, S. Burke, and M. Ernzerhof, *Phys. Rev. Lett.* **77**, 3865 (1996)
- ³⁵ P.E. Blöchl, O. Jepsen, and O.K. Andersen, *Phys. Rev. B* **49**, 16223 (1994)
- ³⁶ R. F. W. Bader, *Atoms in Molecules: A Quantum Theory*, International Series of Monographs on Chemistry (Clarendon Press, Oxford, 1990)
- ³⁷ G. Kresse, and D. Joubert, *Phys. Rev. B* **59**, 1758 (1999).
- ³⁸ G. Kresse, and J. Furthmuller, *Phys. Rev. B* **54**, 11169 (1996).
- ³⁹ I. A. Nekrasov, Z. V. Pchelkina, and M. V. Sadovskii, *JETP Lett.* **88**, 144 (2008)
- ⁴⁰ D. J. Singh, *Phys. Rev. B* **78**, 094511 (2008).
- ⁴¹ I. R. Shein, and A. L. Ivanovskii, *JETP Lett.* **89**, 357 (2009).
- ⁴² A.L. Ivanovskii, *J. Structural Chem.* **50**, 539 (2009)
- ⁴³ I.R. Shein, and A.L. Ivanovskii, *Physica B* **405**, 3213 (2010).
- ⁴⁴ A. Subedi, and D. J. Singh, *Phys. Rev. B* **78**, 132511 (2008)
- ⁴⁵ I. A. Nekrasov, and M. V. Sadovskii, arXiv: 1011.1746 (unpublished).
- ⁴⁶ <http://www.physics.ucdavis.edu/~mindlab>
- ⁴⁷ J. Kortus, I. I. Mazin, K. D. Belashchenko, V. P. Antropov, and L.L. Boyer, *Phys. Rev. Lett.* **86**, 4656 (2001).
- ⁴⁸ B. P. Allen, W. E. Pickett, and H. Krakauer, *Phys. Rev. B* **37**, 7482 (1988).
- ⁴⁹ A. Subedei, D.J. Singh, and M.H. Du, *Phys. Rev. B* **78**, 060506 (2008).
- ⁵⁰ I. R. Shein, and A. L. Ivanovskii, *J. Structural Chem.* **50**, 552 (2009)
- ⁵¹ T. Yildirim, *Phys. Rev. Lett.* **102**, 037003 (2009).
- ⁵² T. Klimczuk, T. M. McQueen, A. J. Williams, Q. Huang, F. Ronning, E. D. Bauer, J. D. Thompson, M. A. Green, and R. J. Cava, *Phys. Rev. B* **79**, 012505 (2009).
- ⁵³ I. R. Shein, and A. L. Ivanovskii, *JETP Lett.* **89**, 285 (2009).
- ⁵⁴ M. J. Mehl, *Phys. Rev. B* **47**, 2493 (1993).
- ⁵⁵ J.F. Nye, *Physical Properties of Crystals*, Oxford University Press, Oxford, 1985.
- ⁵⁶ Z. Wu, E. Zhao, H. Xiang, X. Hao, X. Liu, and J. Meng, *Phys. Rev. B* **76**, 054115 (2007).
- ⁵⁷ R. Hill, *Proc. Phys. Soc. London A* **65**, 349 (1952).
- ⁵⁸ D.H. Chung, *Philos. Mag.* **8**, 833 (1963).
- ⁵⁹ G. Grimvall, *Thermophysical Properties of Materials*, North-Holland, Amsterdam, 1986.
- ⁶⁰ S.F. Pugh, *Philos. Mag.* **45**, 823 (1953).
- ⁶¹ P. Ravindran, L. Fast, P.A. Korzhavyi, B. Johnsson, J.Wills, O. Eriksson, *J. Appl. Phys.* **84** (1998) 4891.
- ⁶² V. Tvergaard, J.W. Hutchinson, *J. Amer. Chem. Soc.* **71** (1998) 157.
- ⁶³ S. I. Ranganathan, and M. Ostoja-Starzewski, *Phys. Rev. Lett.* **101**, 055504 (2008)
- ⁶⁴ I. R. Shein, and A. L. Ivanovskii, *Scripta Mater.* **59**, 1099 (2008).
- ⁶⁵ M. Mito, M. J. Pitcher, W. Crichton, G. Garbarino, P. J. Baker, S. J. Blundell, P. Adamson, D. R. Parker, and S. J. Clarke, *J. Am. Chem. Soc.* **131**, 2986 (2009).
- ⁶⁶ I. R. Shein, and A. L. Ivanovskii, *Tech. Phys. Lett.* **35**, 961 (2009).
- ⁶⁷ M. Aftabuzzaman, A. K. M. A. Islam, and S.H. Naqib, arXiv:0909.2914 (unpublished).
- ⁶⁸ I. R. Shein, and A. L. Ivanovskii, *Physica C* **469**, 15 (2009).
- ⁶⁹ A. Martinelli, M. Ferrett, A. Palenzona, and M. Merlini, *Physica C* **469**, 782 (2009).

TABLE I. The optimized lattice parameters (a and c , in Å), internal coordinates ($z_{\text{Sr,Pt,As}}$), some inter-atomic distances (d , in Å), and total-energy differences (ΔE , eV/cell) for the examined SrPt_2As_2 polymorphs.

phase/parameter *	SPA-I	SPA-II	SPA-III
a	4.5279/4.5135 (4.46-4.51) **	4.5218/4.5440	4.6428/4.6761
c	10.0137/10.0549 (9.81) **	10.1957/10.1852	9.7329/9.6393
c/a	2.2116/2.2277	2.2548/2.2415	2.0963/2.0614
$z_{\text{Sr,As,Pt}}$	$z_{\text{Sr}}=0.2504/0.2501$ $z_{\text{Pt}}=0.3810/0.3798$ $z_{\text{As}}=0.1286/0.1295$	$z_{\text{As}}=0.3675/0.3665$	$z_{\text{Pt}}=0.3599/0.3564$
d^1	2.60/2.61 (Pt-As in $[\text{Pt}_2\text{As}_2]$) 2.56/2.56 (Pt-As in $[\text{As}_2\text{Pt}_2]$)	2.56/2.57 (Pt-As in $[\text{Pt}_2\text{As}_2]$) 4.00/4.01 (As-As in $[\text{Pt}_2\text{As}_2]$)	2.78/2.76 (Pt-As in $[\text{As}_2\text{Pt}_2]$) 3.91/3.89 (Pt-Pt in $[\text{As}_2\text{Pt}_2]$)
d^2	2.52/2.52 (Pt-As)	2.70/2.70 (As-As)	2.76/2.78 (Pt-Pt)
ΔE	0	0.46/0.42	0.20/0.16

* as obtained within FLAPW/VASP

** available experimental data (Ref. [31]) are given in parentheses

d^1 are the labeled inter-atomic distances inside $[\text{Pt}_2\text{As}_2]$ ($[\text{As}_2\text{Pt}_2]$) blocks

d^2 are the nearest Pt-As (As-As, or Pt-Pt) distances between neighboring blocks: $[\text{Pt}_2\text{As}_2]/[\text{As}_2\text{Pt}_2]$ ($[\text{Pt}_2\text{As}_2]/[\text{Pt}_2\text{As}_2]$ or $[\text{As}_2\text{Pt}_2]/[\text{As}_2\text{Pt}_2]$)

TABLE II. Calculated bond angles in $\{\text{PtAs}_4\}$ ($\{\text{AsPt}_4\}$) tetrahedrons for the examined SrPt_2As_2 polymorphs.

phase/parameter *		SPA-I	SPA-II	SPA-III
$\{\text{PtAs}_4\}$	As-Pt-As	104.2/104.5	102.7/102.5	
	Pt-As-Pt	120.7/120.0	124.2/124.5	
		75.8/75.5	77.3/77.5	
$\{\text{AsPt}_4\}$		120.7/120.0	124.4/124.5	
	As-Pt-As	77.4/77.1		79.7/80.7
	Pt-As-Pt	124.4/123.6		130.0/133.0
		102.6/102.9		100.3/99.1
		124.4/123.6		130.0/133.0

* as obtained within FLAPW/VASP

TABLE III. Total (in states/eV·f.u.) and partial (in states/eV·atom) densities of states at the Fermi level, electronic heat capacity γ (in $\text{mJ}\cdot\text{K}^{-2}\cdot\text{mol}^{-1}$), and molar Pauli paramagnetic susceptibility χ (in $10^{-4} \text{emu}\cdot\text{mol}^{-1}$) for the examined SrPt_2As_2 polymorphs.

phase/parameter	As 4 p	Pt 5 d	total	γ	χ
SPA-I	0.11/0.16 *	0.59/0.30 *	2.55	6.01	0.82
SPA-II	0.22	0.73	2.06	4.86	0.66
SPA-III	0.17	0.46	1.69	3.98	0.54

* for non-equivalent atoms: $(\text{Pt}^1, \text{As}^1)/(\text{Pt}^2, \text{As}^2)$; see Sec. II.

TABLE IV. Fermi velocity along different directions ($\langle v_{x,y,z}^2 \rangle^{1/2} \times 10^7 \text{ cm/s}$) for the examined SrPt_2As_2 polymorphs in comparison with some others layered SCs.

phase	$\langle v_x^2 \rangle^{1/2}$	$\langle v_y^2 \rangle^{1/2}$	$\langle v_z^2 \rangle^{1/2}$
SPA-I	2.47	2.47	1.62
SPA-II	1.93	1.93	1.87
SPA-III	2.12	2.12	1.95
MgB_2 *	4.90	4.90	4.76
$\text{La}_{1.85}\text{Sr}_{0.15}\text{CuO}_4$ **	2.2	2.2	0.41
$\text{YBa}_2\text{Cu}_3\text{O}_7$ **	1.8	2.8	0.7

* Ref. [47].

** Ref. [48].

TABLE V. Effective atomic charges (in e) for SrPt_2As_2 polymorphs as obtained from a purely ionic model (Q^i), Bader analysis (Q^B), and their differences ($\Delta Q = Q^B - Q^i$).

phase/parameter	Q	Pt	As	Sr
	Q^i	+2	-3	+2
SPA-I	Q^B	10.565/10.894 *	4.938/5.004 *	8.599
	ΔQ	2.565/2.894 *	-3.063/-2.996 *	0.599
	Q^i	+2	-3	+2
SPA-II	Q^B	10.684	5.023	8.587
	ΔQ	2.684	-2.973	0.587
	Q^i	+2	-3	+2
SPA-III	Q^B	10.760	4.952	8.577
	ΔQ	2.760	-3.048	0.577

* for non-equivalent atoms: $(\text{Pt}^1, \text{As}^1)/(\text{Pt}^2, \text{As}^2)$; see Sec. II.

TABLE VI. Calculated elastic constants (C_{ij} , in GPa) for SrPt₂As₂ tetragonal polymorphs.

phase/parameter	SPA-I	SPA-II	SPA-III
C_{11} *	136	132	165
C_{12}	66	22	57
C_{13}	89	56	69
C_{33}	148	109	139
C_{44}	30	31	25
C_{66}	17	< 5	27

* as obtained within VASP

TABLE VII. Calculated elastic parameters for SrPt₂As₂ polymorphs: bulk moduli (B , in GPa), compressibility (β , in GPa⁻¹), shear moduli (G , in GPa), Pugh's indicator (G/B), Young's moduli (Y , in GPa), Poisson's ratio (ν), and the so-called universal anisotropy index (A^U).

Phase/parameter *	SPA-I	SPA-II	SPA-III
B_V	101	71	95
B_R	99	71	95
B_{VRH}	100	71	95
β	0.010	0.014	0.010
G_V	27	29	34
G_R	25	5	30
G_{VRH}	26	17	32
G/B	0.26	0.24	0.34
Y	72	46	87
ν	0.38	0.39	0.35
A^U	0.42	-5.83	-5.12

* as obtained within VASP

Figures

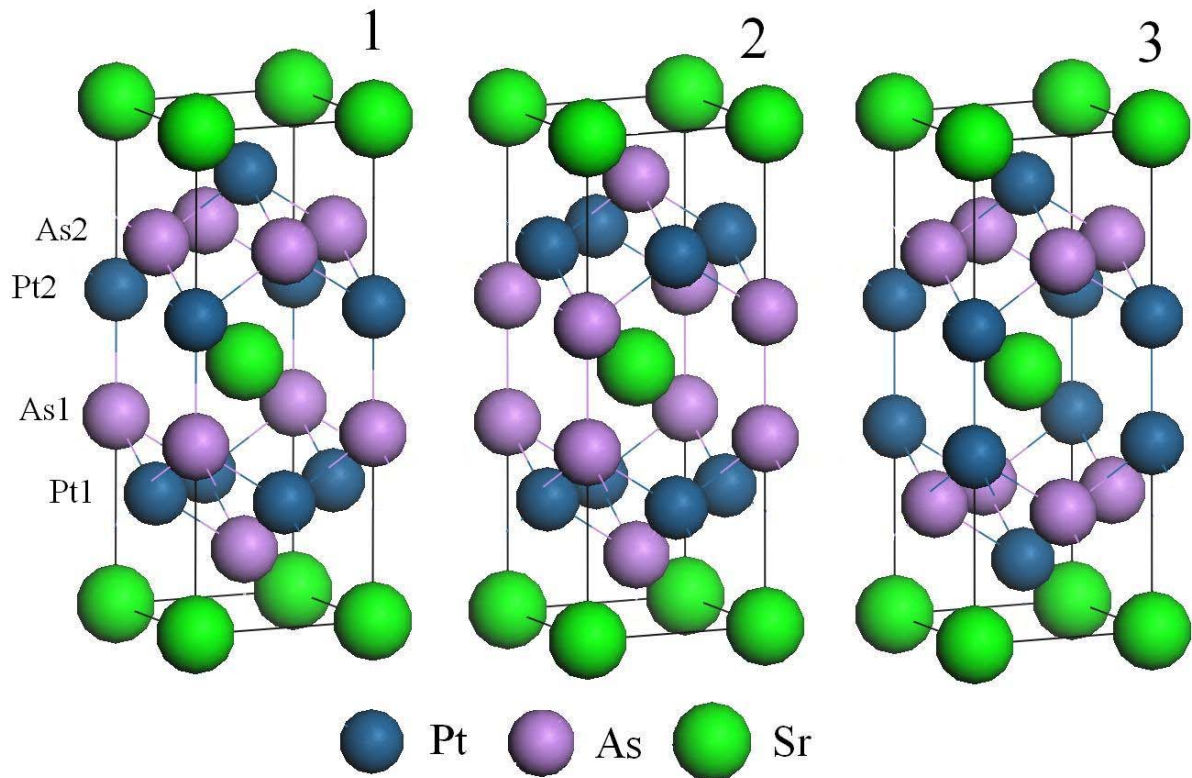


FIG. 1. (*Color online*) Crystal structures of the examined SrPt_2As_2 polymorphs: (1) SPA-I, (2) SPA-II, and (3) SPA-III (*see text*).

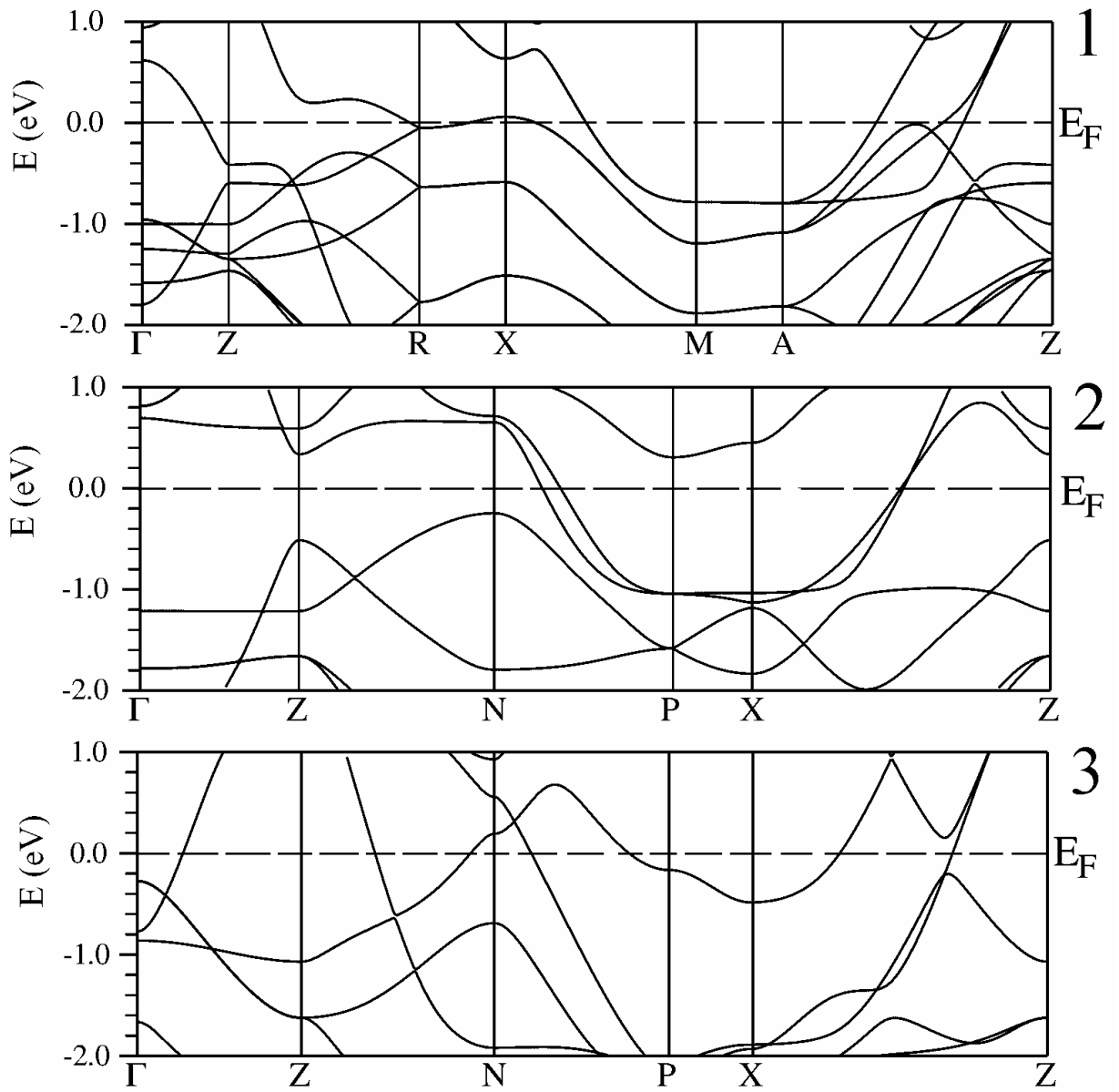


FIG. 2. Electronic band structures of SrPt₂As₂ polymorphs: (1) SPA-I, (2) SPA-II, and (3) SPA-III.

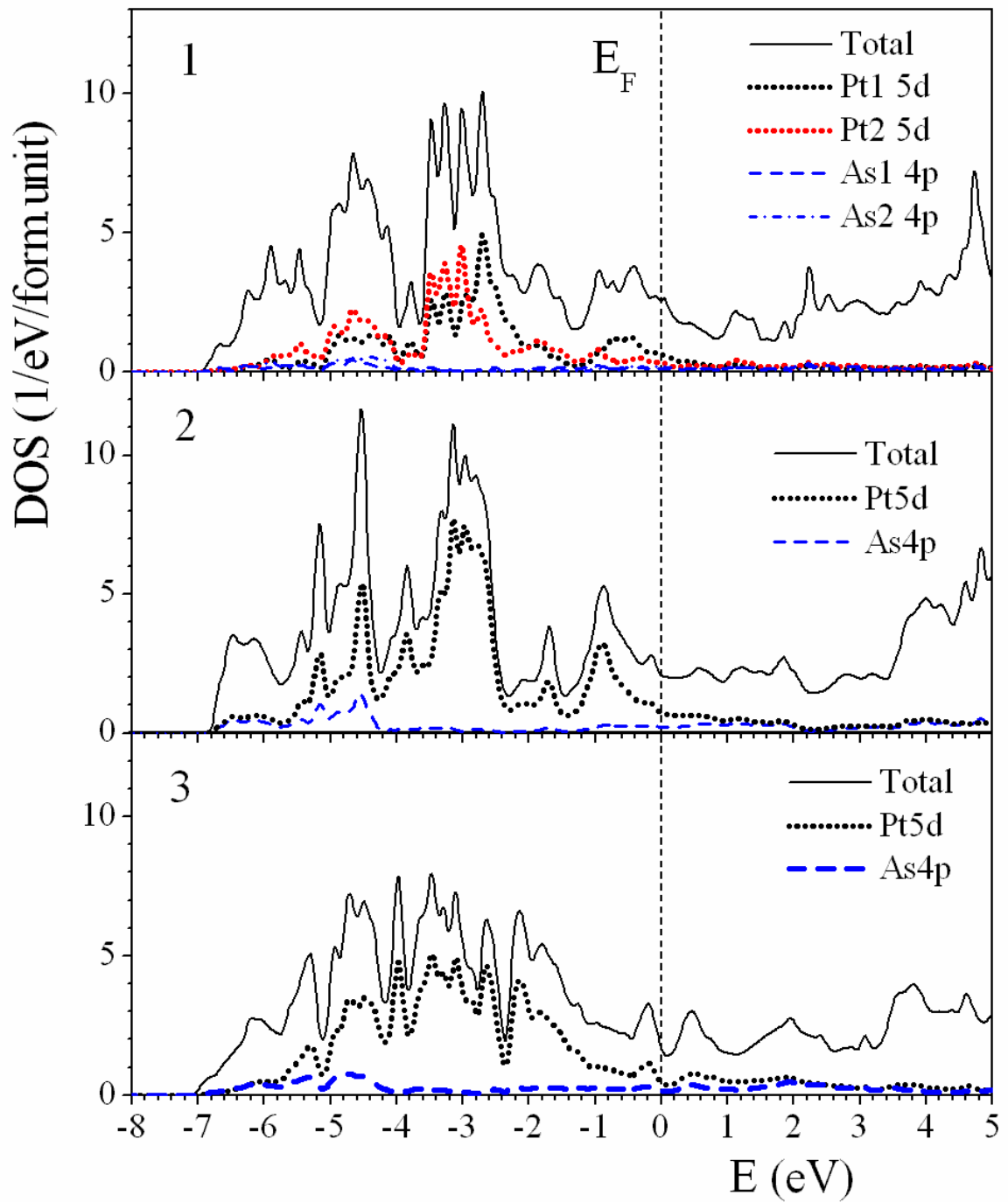


FIG. 3. (Color online) Total and partial densities of states of SrPt_2As_2 polymorphs: (1) SPA-I, (2) SPA-II, and (3) SPA-III.

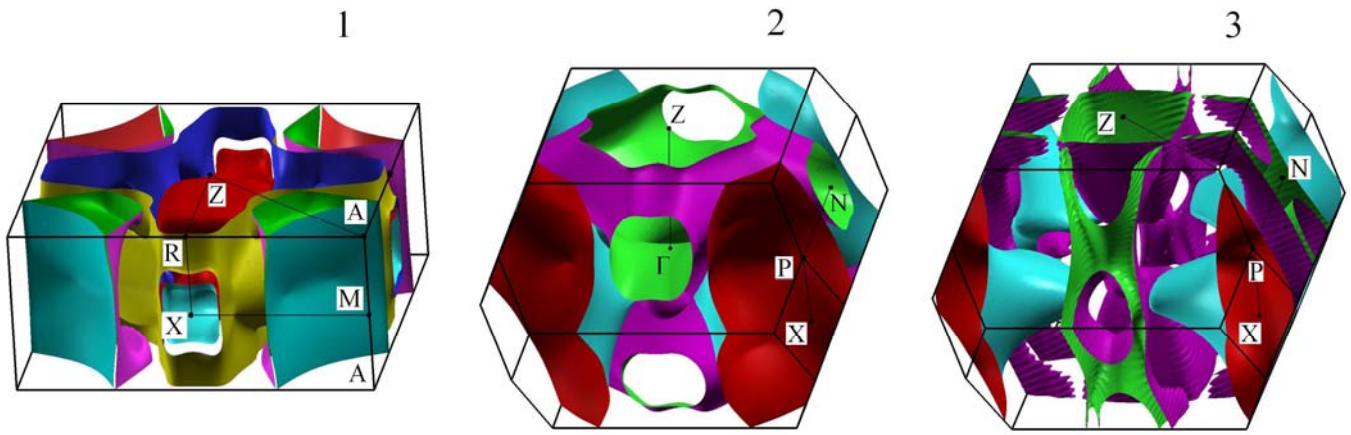


FIG. 4. (*Color online*) The Fermi surfaces of SrPt_2As_2 polymorphs: (1) SPA-I, (2) SPA-II, and (3) SPA-III.

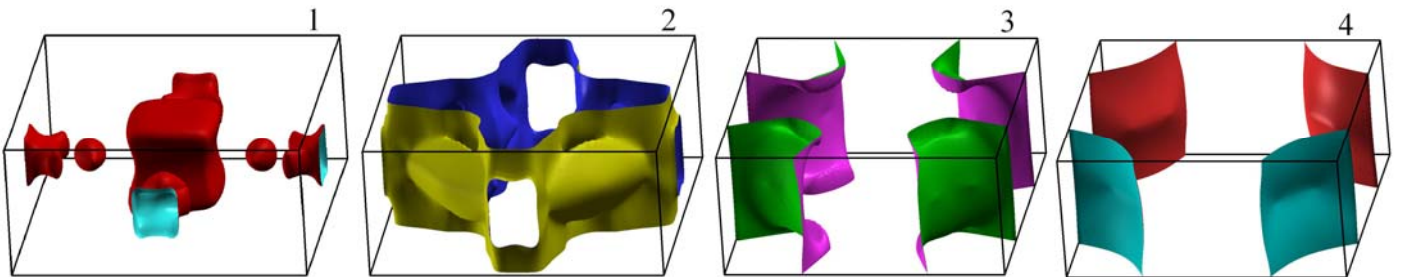


FIG. 5. (*Color online*) Separate sheets of the Fermi surface for CaBe_2Ge_2 -like SrPt_2As_2 . Three of them (2, 3, and 4) are electronic-like, and sheet 1 is hole-like, see also Ref. [45].

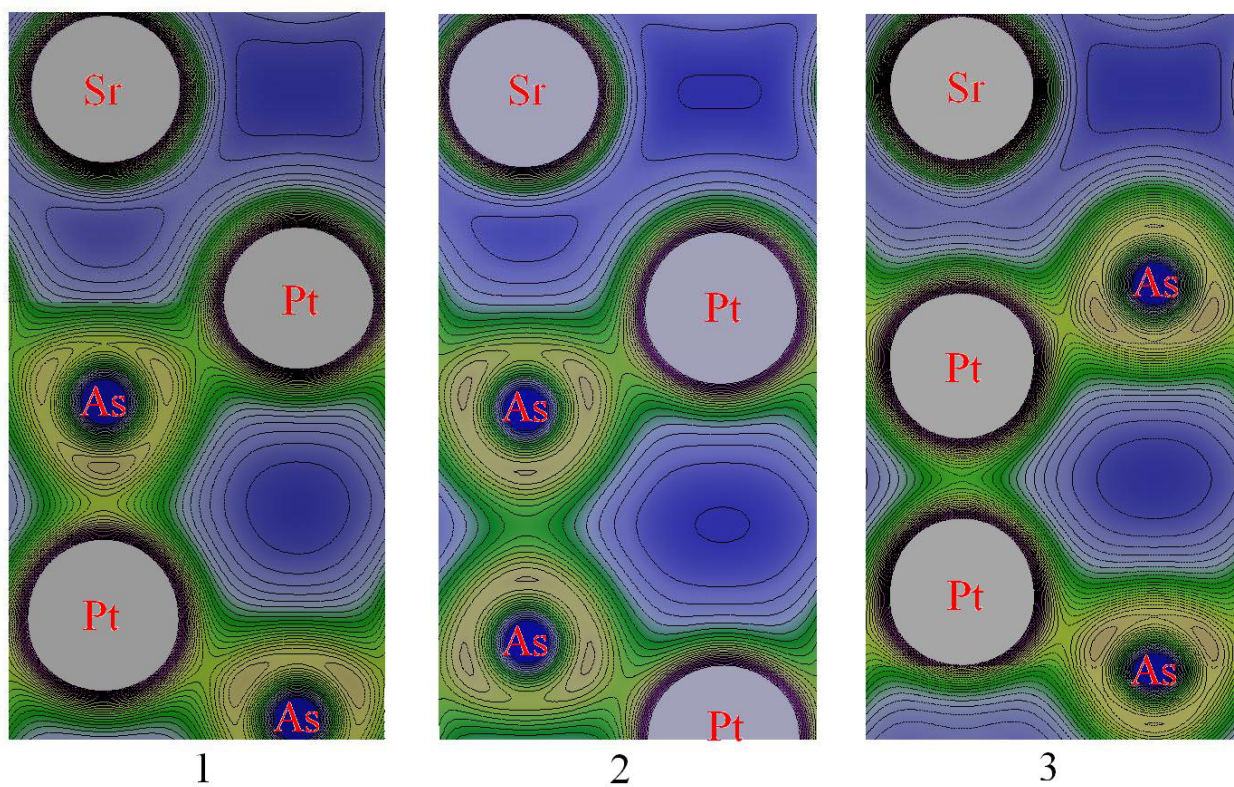


FIG. 6. (*Color online*) Charge density maps of SrPt₂As₂ polymorphs illustrating the formation of directional "inter-blocks" covalent bonds: (1) As-Pt bonds for SPA-I, (2) As-As bonds for SPA-II, and (3) Pt-Pt bonds –for SPA-III.